Supporting Information

A Eutectic Salt-assisted Semi-closed Pyrolysis Route to Fabricate High-density Active-sites Hierarchically Porous Fe/N/C Catalysts for Oxygen Reduction Reaction

Jia Li[a], Siguo Chen*[,a], Wei Li[a], Rui Wu[a], Shumaila Ibraheem[a], Jing Li[a], Wei Ding[a], Li Li[a], and Zidong Wei*[,a]

[a]*The State Key Laboratory of Power Transmission Equipment & System Security and New Technology; Chongqing Key Laboratory of Chemical Process for Clean Energy and Resource Utilization, College of Chemistry and Chemical Engineering, Chongqing University, Chongqing 400044, China.*

**E-mail: csg810519@126.com, zdwei@cqu.edu.cn*

Experimental Section

Preparation of Fe/N/C-$ZnCl_2$/KCl. 8g $ZnCl_2$ and 8g KCl were dispersed in 50 mL deionized water at room temperature for 10 min. The mixture was then immediately frozen via direct injection into liquid nitrogen. In the liquid nitrogen, the samples were kept for additional 5 minutes. Then the samples were placed into a freeze dryer at <0.05 mbar for 60 to 72h. 2.5g $FeCl_3 \cdot 6H_2O$ was dissolved in 1 mL ethanol and 1g *o*PD (o-phenylenediamine) was dissolved in 12 mL ethanol. After that *o*PD solution was added into $FeCl_3 \cdot 6H_2O$ solution to form dark magenta precipitate. Then, the mixture was dropwise added into the $ZnCl_2$/KCl eutectic salt with continuous grinding for 1 h, to which 2.5g $NH_4S_2O_8$ dissolved HCl (1M, 4 mL) solution was added. After another 1 h grinding and 24h quiet placing, the resulting brown mixture was transferred into a muffle furnace, and heated at 150°C for 2 h. The sample was cooled to room temperature, and then heated to 800°C at a heating rate of 5°C/min and held at 800°C for 2 hours under flowing N_2. The obtained black powder was washed with 1 M HCl solution at 80°C for 8 h followed by centrifugation, washing and freeze-drying. Before achieving the final products, the precursors were carbonized for the second time at 900°C for 2 h with a heating rate of 5°C/min under flowing N_2. For comparison, *Fe/N/C-KCl* catalyst was prepared under similar conditions as those mentioned above.

Preparation of Fe/N/C-$ZnCl_2$. For the synthesis of Fe/N/C-$ZnCl_2$, 8g $ZnCl_2$ was dissolved in 20 mL deionized water at room temperature for 10 min. 2.5g $FeCl_3 \cdot 6H_2O$ was dissolved in 1 mL ethanol and 1g *o*PD (o-phenylenediamine) was dissolved in 12 mL ethanol, respectively. The precursor solution was obtained by a quickly mixing of

*o*PD, $FeCl_3 \cdot 6H_2O$ and $ZnCl_2$ solutions to form dark magenta precipitate. The reaction mixture was stirred for 2 hours at 0°C. Next, 2.5g $NH_4S_2O_8$ dissolved HCl (1M, 4mL) solution was added slowly into this mixture with moderate stirring for 2 h under 0°C. After another 24 h of vigorous stirring under room temperature, the mixture was then transferred to glass petri dishes and allowed to slowly evaporate under ambient conditions for 24 h. The resulting brown mixture was transferred into a muffle furnace, heated at 150°C for 2 h. After cooling to room temperature, the temperature was raised to 800°C at a heating rate of 5°C/min and held at 800°C for 2 hours under flowing N_2. The obtained black powder was washed with 1 M HCl solution at 80°C for 8 h followed by centrifugation, washing and freeze-drying. Before achieving the final products, the precursors were carbonized for the second time at 900°C for 2 h with a heating rate of 5°C/min under flowing N_2. For comparison, *Fe/N/C* catalyst was prepared under the conditions similar to those mentioned above.

The final yield is calculated according the equation below:

$$\text{Final yields of catalysts} = \frac{\text{Final weight of catalysts}}{\text{Initial weight of oPD}}$$

Electrochemical measurements.

All electrochemical experiments were performed in a standard three-electrode cell at room temperature. The cell consisted of a glassy carbon working electrode (GC electrode, 5 mm in diameter, PINE: AFE3T050GC), an Ag/AgCl (3M KCl) reference electrode, and a graphite rod counter electrode. All potentials in this study, however, are given relative to a reversible hydrogen electrode (RHE). The working electrodes were prepared by applying catalyst ink onto glassy carbon (GC) disk electrodes. To

obtain a catalyst ink, 4 mg of the as-prepared Fe/N/C catalysts and 10 μL of 5 wt% Nafion solution (Dupont) were dispersed in 400 μL of ethanol by at least 30 min sonication to form a homogeneous ink. For preparing the working electrode, the glassy carbon (GC) electrode was pre-polished with 300 and 50 nm alumina slurries for several minutes, then 10 μL of the catalyst ink was drop-coated on the rotation disk electrode (RDE) or rotation ring-disk electrode (RRDE) surface (5 mm in diameter, Pine Instruments), giving a mass loading of 0.5 mg cm^{-2}. Commercial 20 wt% platinum on Vulcan carbon black (Pt/C) was measured for comparison. The working electrode was prepared as follows, 2 mg Pt/C and 10 μL of 5 wt% Nafion solution (Dupont) were dispersed in 800 μL of ethanol by at least 30 min sonication to form a homogeneous ink. 10 μL of catalyst ink was then pipetted onto the GC surface, leading to a Pt loading of 5 μg cm^{-2}. After drying at room temperature, a drop of 0.01 wt% Nafion solution (Dupont) was applied onto the surface of the catalyst layer to form a thin protective film. The prepared electrodes were dried at room temperature before the electrochemical tests. All of the electrodes were pretreated by cycling the potential between 0 and 1.2 V at a sweep rate of 50 mV s^{-1} for 50 cycles in order to remove any surface contamination prior to ORR activity testing. The activities of catalysts were performed by recording linear sweep voltammetry (LSV) curves in the oxygen-saturated 0.1 M KOH or 0.1 M $HClO_4$ solution. The LSV curves for ORR were recorded at potential scan rate of 10 mV s^{-1}. The rotation speed was controlled at 1,600 rpm. The ORR data was substracted by the background current in N_2-saturated electrolyte and the ORR curves were iR-corrected.

RRDE experiments: RRDE measurements were conducted at 25℃ in an oxygen-saturated 0.1 M $HClO_4$ solution at a scan rate of 10 mV s^{-1} and a rotation speed of 1600 rpm. (Pine Instrument). The catalyst loaded carbon cloth with 0.5 mg cm^{-2} was used as the working electrode for studying the ORR stability. The carbon cloth was pre-treated in the solution of dilute hydrochloric acid, dilute alkali and ethanol ultrasounding for 1 minute at room temperature to remove organic contaminants and hydroxylate the surface before loading the catalyst. Total electron-transfer number (n) and hydrogen peroxide yield ($\%H_2O_2$) were determined by RRDE approach using

$$n = \frac{4I_{disk}}{I_{ring} / N + I_{disk}} \quad (1)$$

$$\%H_2O_2 = \frac{2I_{ring} / N}{I_{ring} / N + I_{disk}} \times 100\% \quad (2)$$

where I_{disk} and I_{ring} are the voltammetric currents at the disk and ring electrode, respectively. N is the RRDE collection efficiency, which was determined to be ~37%.

Electrochemical impedance spectroscopy (EIS) measurements were recorded in O_2-saturated 0.1 M $HClO_4$ at 0.80 V vs. RHE with 10 mV ac potential from 10 kHz to 0.01 Hz. The loading was 0.5 mg cm^{-2} for all materials. Electrode rotation speed, 1,600 rpm.

MEAs preparation and PEMFC tests. The catalyst ink was prepared by ultrasonically mixing the catalyst powder with 5 wt% Nafion solution (DuPont) and anhydrous alcohol for approximately 10 min. The Nafion content in the dry catalyst layer was 33 wt%. The suspension was pipetted onto the gas diffusion layer and finally heated at 60℃ for 2 hours. The weight difference was measured and used to calculate the loading of the catalysts. A suspension consisting of 40 wt% Pt/C catalysts (Johnson-

Matthey In. UK), 5 wt% Nafion solution (DuPont) (25 wt% in the catalyst layer), and anhydrous alcohol was used to prepare the anode. The Pt loading was controlled at 0.3 mg cm^{-2} on the anodic side. The MEA was prepared by hot-pressing the cathode, Nafion 112 membrane (DuPont), and the anode at 137℃ and 5 MPa for 2 min. The Nafion 112 membrane was pretreated with 3 vol. % H_2O_2 and 0.5 M H_2SO_4 for 1 h to remove impurities. The membrane was then washed several times with hot ultrapure water. Pure hydrogen and oxygen were supplied to the anode and cathode at a flow rate of 250 and 300 sccm, respectively. The MEA was measured by a fuel cell test station (Fuel Cell Technologies, Inc) with UHP-grade H_2 and O_2 at 80 °C. All the gases were humidified at 80 °C with the flow rate of 0.25 L min^{-1} for H_2 and 0.3 L min^{-1} for O_2. The absolute pressures of H_2 and O_2 were the same and set at 2.0 bar.

Zn-O_2 batteries tests. The Zn-O_2 battery was fabricated using a self-made plastic cell. The gas diffusion layer (GDL) was made by transferring a certain volume of 10 wt% polytetrafluoroethylene (PTFE) emulsion (60 wt%, Saibo electrochemical) onto the back of a cleaned carbon paper. The carbon paper was transferred into a muffle furnace, heated at 350℃ for 2 h. Subsequently, the O_2 electrode was made by transferring a certain volume of catalyst ink onto the carbon paper substrate with a catalyst loading of 0.5 mg cm^{-2}. A polished zinc foil (0.5 mm thickness) was used as the anode. The area of the electrodes exposed to the electrolyte is 1.0 cm^2. A Ni foam was used as current collector. The electrolyte was 6.0 M KOH to ensure reversible zinc electrochemical reactions at the Zn anode.

Battery test: All the Zn-O_2 batteries were tested under ambient atmosphere. The

olarization curve measurements were performed by LSV (5 mV s^{-1}) at 25℃ with VersaSTAT 4 electrochemical working station. Both the current density and power density were normalized to the effective surface area of O_2 electrode. The specific capacity was calculated according the equation below:

$$\frac{current * service\ hours}{weight\ of\ consumed\ zinc} \tag{3}$$

The energy density was calculated according the equation below:

$$\frac{current * service\ hours * average\ discharge\ voltage}{weight\ of\ consumed\ zinc} \tag{4}$$

The galvanostatic discharge was carried out by LAND testing system.

Characterization.

SEM test: Scanning electron microscope (SEM) was obtained using a JSM-7800F (JEOL) field emission scanning electron microscope operated at an acceleration voltage of 15 kV.

TEM and STEM test: Low-resolution transmission electron microscopy (TEM) was carried out on a FEI Tecnai G2 20S-TWIN instrument operating at 120 kV. High-resolution transmission electron microscopy (HRTEM) was carried out on a JEM-2100 instrument operating at 200 kV. High-angle annular dark-field scanning transmission electron microscope (HAADF-STEM)-energy-dispersive X-ray spectroscopy (EDS) were taken on a TecnaiG2F20S-TWIN transmission electron microscope operated at 200 kV.

Raman spectrum test: Raman spectrum was recorded by a LabRamHR evolution Raman spectrometer equipped with a Nb-Yag laser excitation source operating at 532

nm.

TGA/DTA test: TGA/DTA was performed on a Mettler TGA/DSC1/1600LF Thermogravimetric Analyzer under nitrogen flow with a heating rate of 5 K min^{-1} in the region 298−1273 K.

XRD test: Powder X-ray diffraction (XRD) data were collected on a PANalytical X' pert diffractometer equipped with a PIXcel 1D detector (Cu Kα radiation, 1.5406 Å). The operation voltage and current were 40 kV and 40 mA, respectively.

BET and pore-size distribution test: The specific surface area of the samples was measured using Brunauer–Emmett–Teller (BET) analysis of their adsorption and desorption isotherms, with experiments conducted at 77 K using a Kubo X1000 aperture and surface area analysis instrument.

XPS test: X-ray Photoelectron Spectroscopy (XPS) was conducted on a ESCALAB250Xi spectrometer equipped with a monochromatic Al X-ray source (Al KR, 1.4866 keV). High-resolution elemental analysis was performed on the C 1s (295–275 eV), N 1s (390–410 eV) regions with a pass energy of 20 eV, a step of 0.05 eV, and an 800 ms dwell time. Each spectrum was constructed from an average of two scans. The pressure in the XPS analysis chamber was maintained at 10^{-7} Pa or lower during collection. In the data analysis, the binding energy (BE) of the core level C 1s peak was set at 284.6 eV to compensate for surface-charging effects. The Shirley background was subtracted, and the satellite peaks were removed for all element peaks before curve fitting. The experimental spectra were fitted into a Gaussian line shape. The surface elemental compositions were determined by the ratios of peak areas that had been

corrected with empirical sensitivity factors.

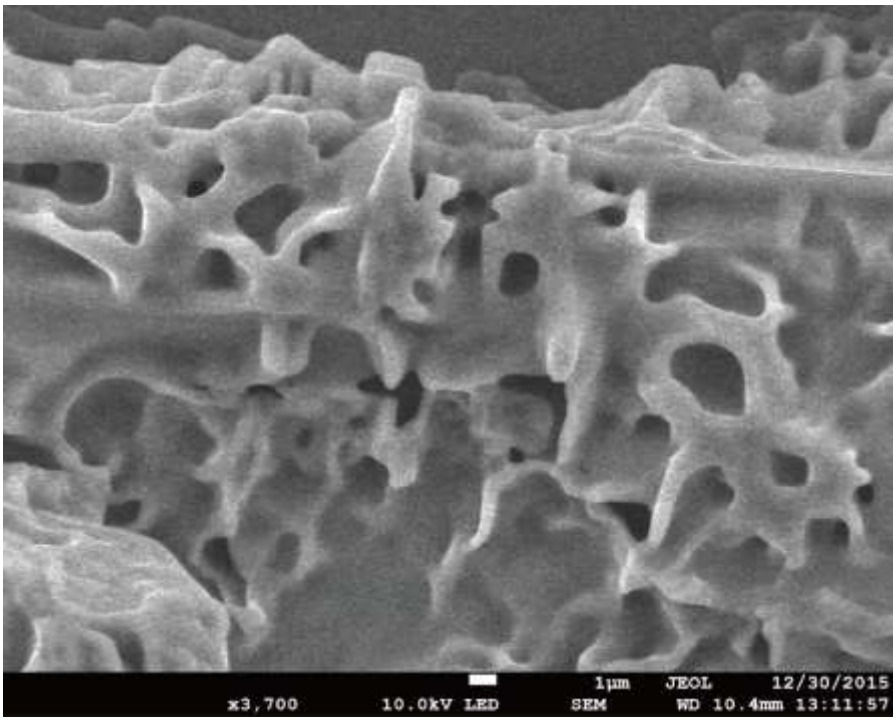

Figure S1. SEM image of 3D porous KCl salt. The SEM image of KCl/$ZnCl_2$ and $ZnCl_2$ cannot obtained because the $ZnCl_2$ is very hygroscopic.

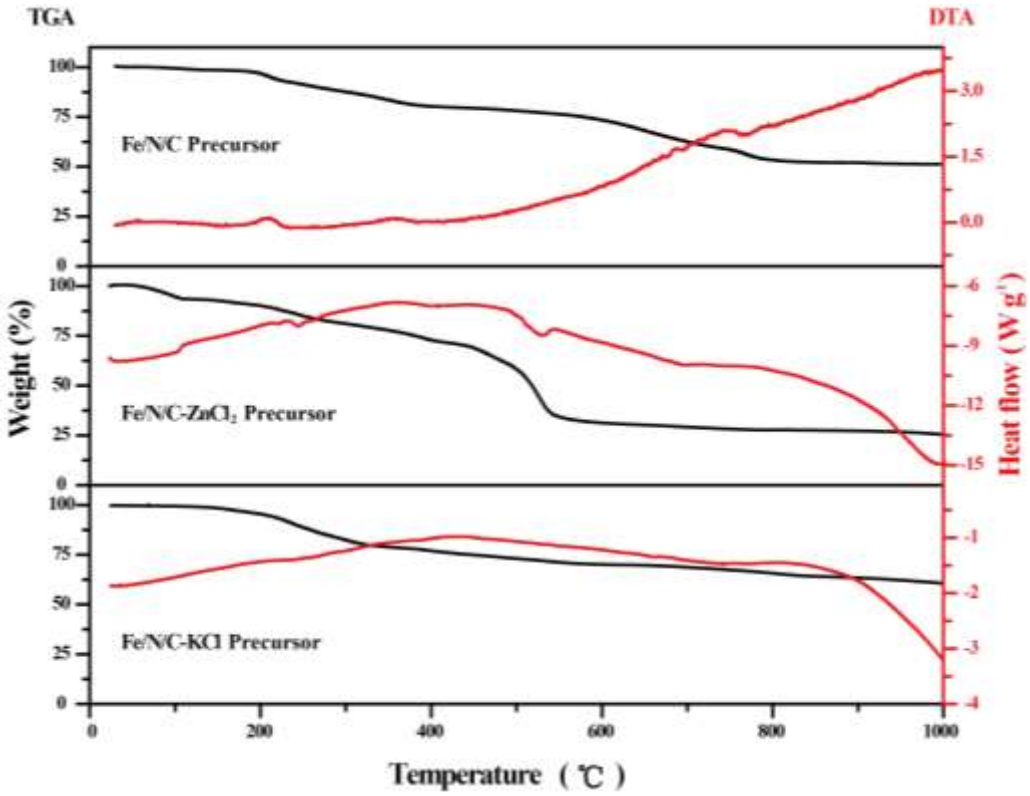

Figure S2. TGA/DTA curves of Fe/N/C, Fe/N/C-$ZnCl_2$ and Fe/N/C-KCl precursors with the heating rate of 5 C° min^{-1} in nitrogen condition.

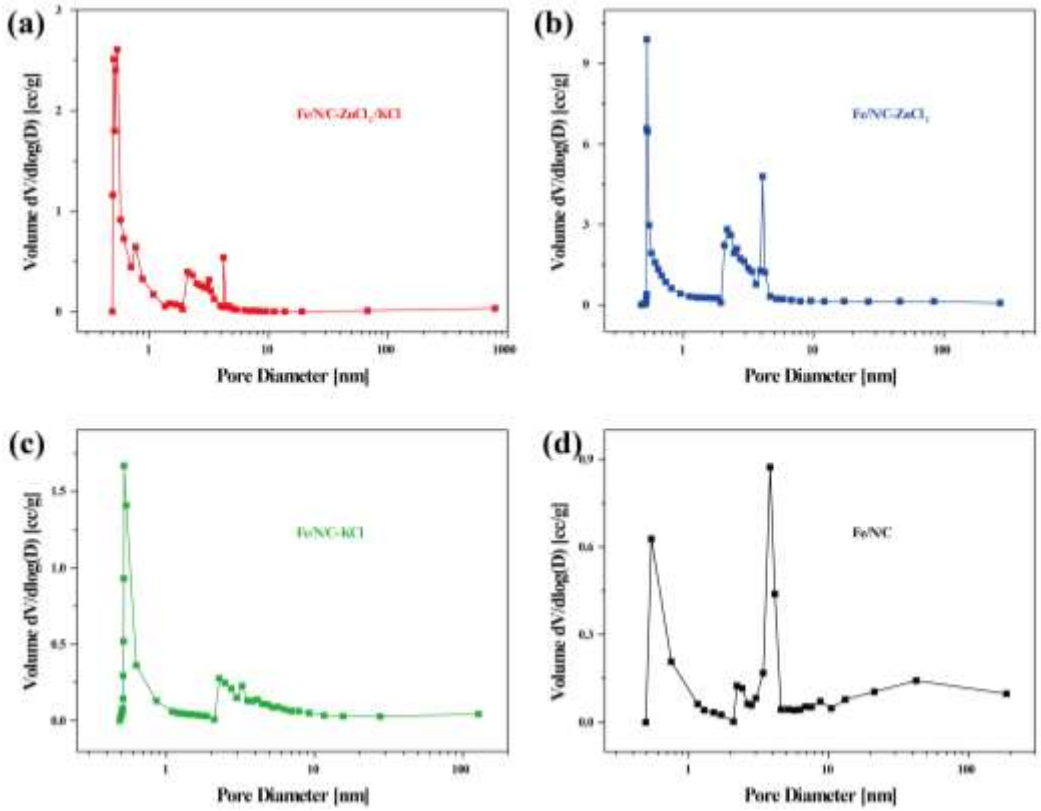

Figure S3. Barrett-Joyner-Halenda (BJH) pore-size distribution analysis of (a) Fe/N/C-$ZnCl_2$/KCl, (b) Fe/N/C-$ZnCl_2$, (c) Fe/N/C-KCl and (d) Fe/N/C catalysts.

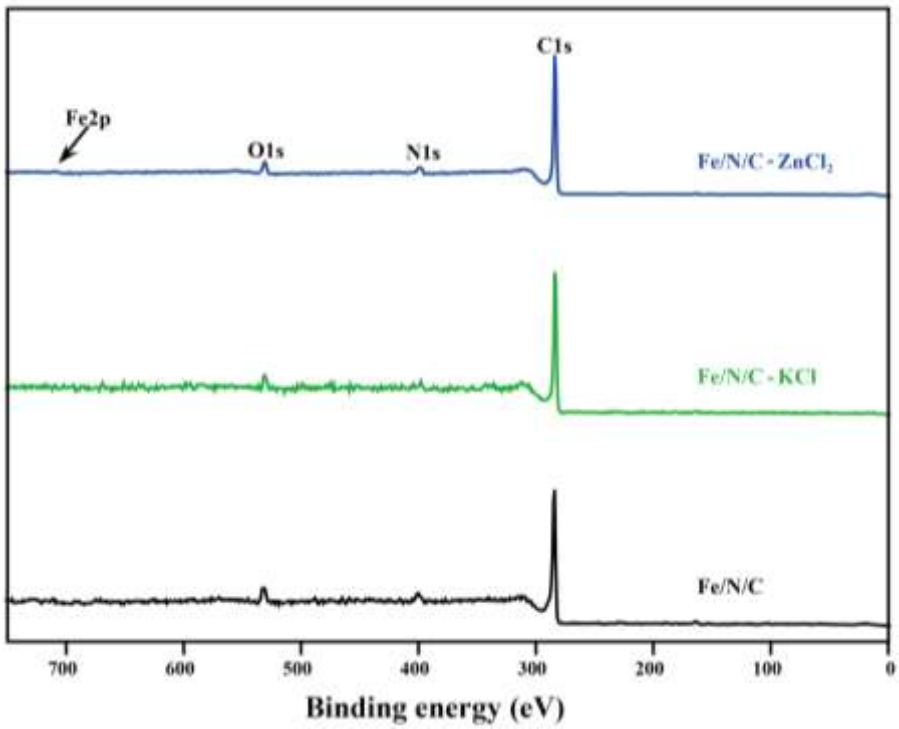

Figure S4. XPS survey spectra of Fe/N/C-$ZnCl_2$, Fe/N/C-KCl and Fe/N/C catalysts.

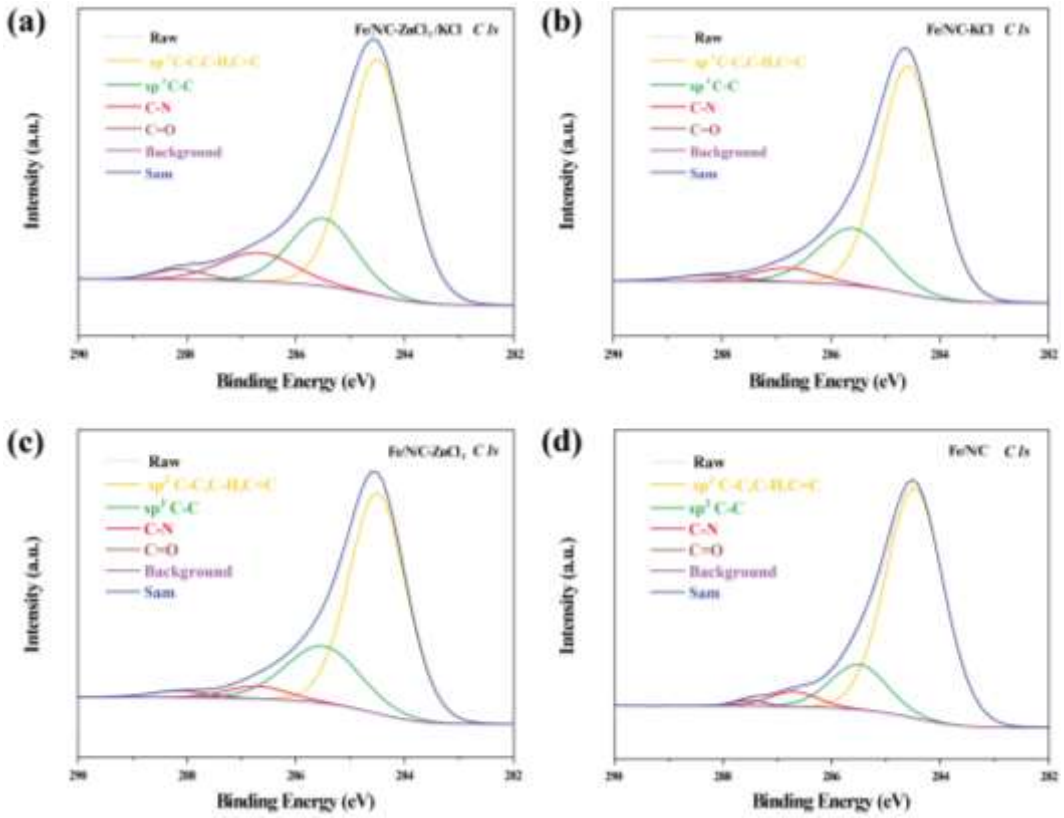

Figure S5. C1s spectra of (a) Fe/N/C-$ZnCl_2$/KCl, (b) Fe/N/C-KCl, (c) Fe/N/C-$ZnCl_2$ and (d) Fe/N/C catalysts.

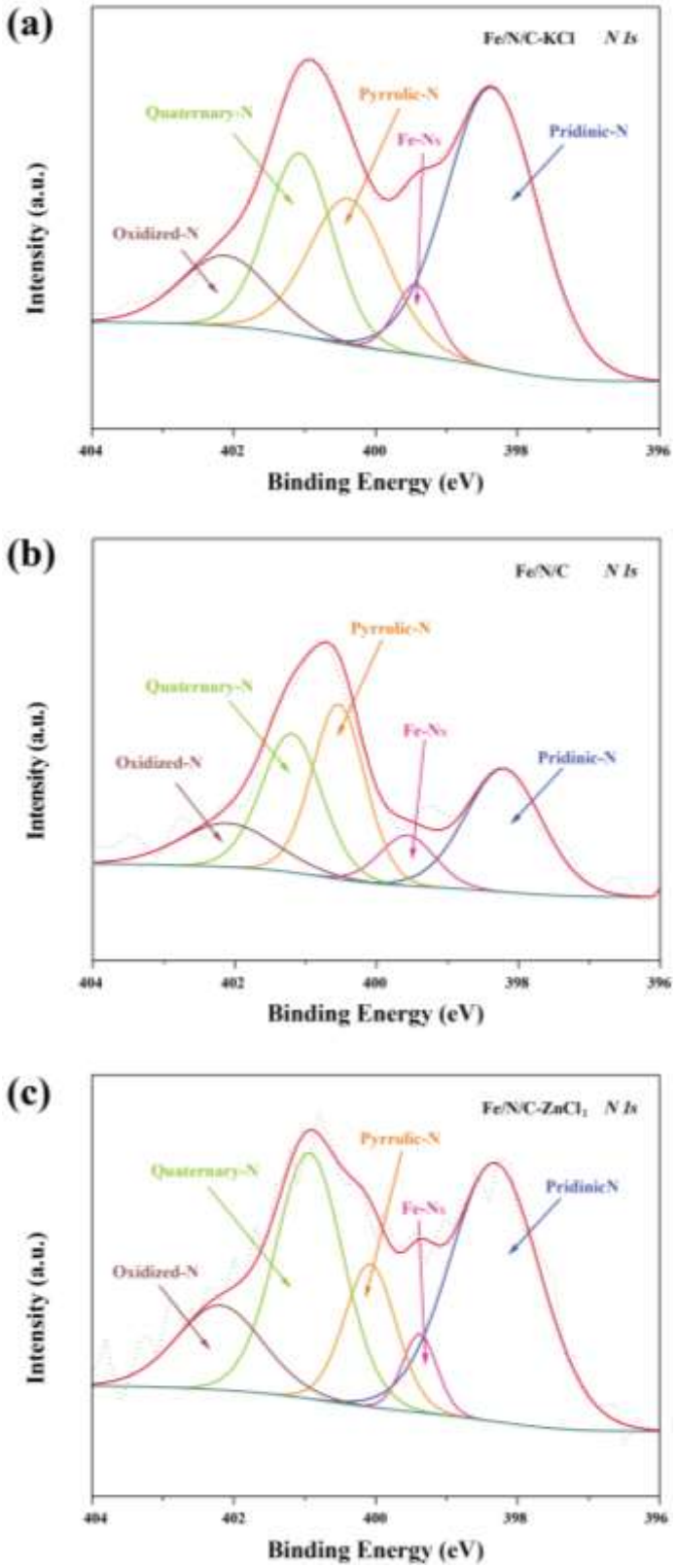

Figure S6. N1s spectra of (a) Fe/N/C-KCl, (b) Fe/N/C and (c) Fe/N/C-$ZnCl_2$ catalysts.

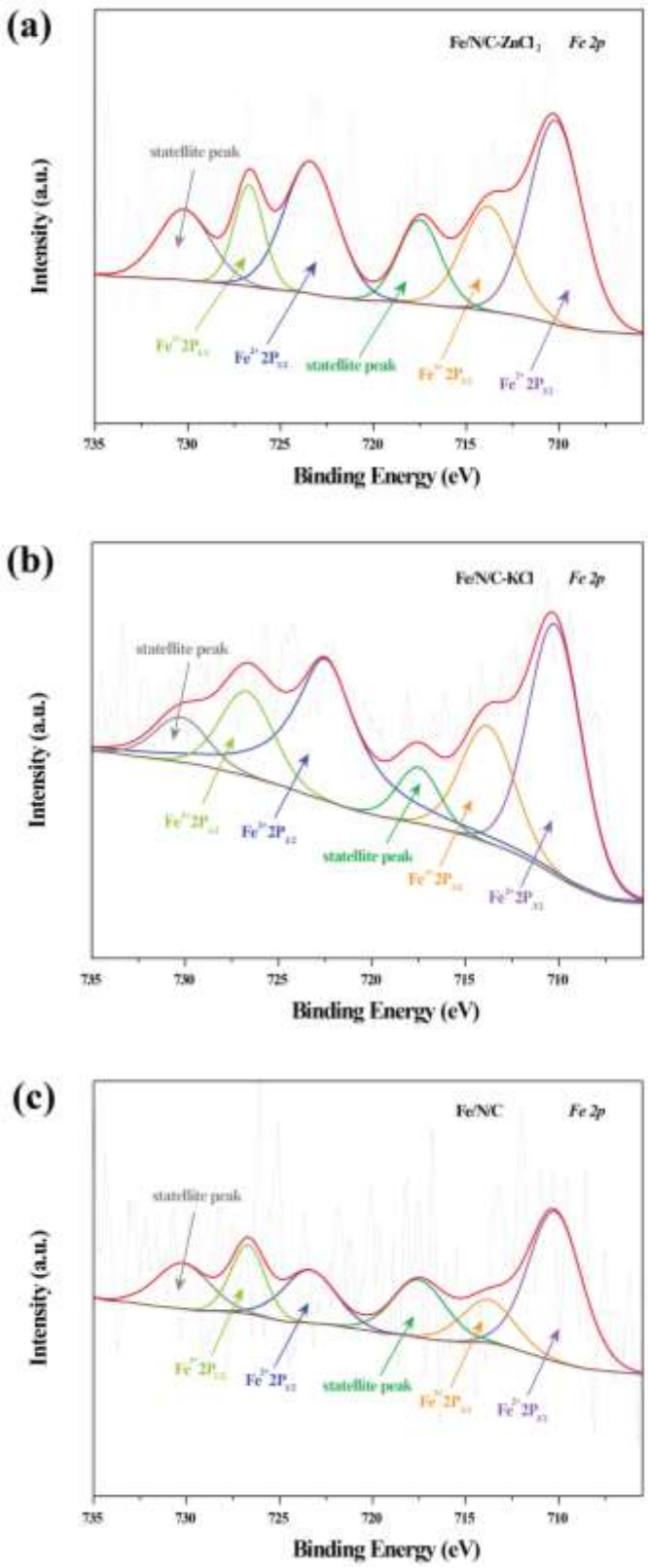

Figure S7. Fe 2p spectra of (a) Fe/N/C-$ZnCl_2$, (b) Fe/N/C-KCl and (c) Fe/N/C catalysts.

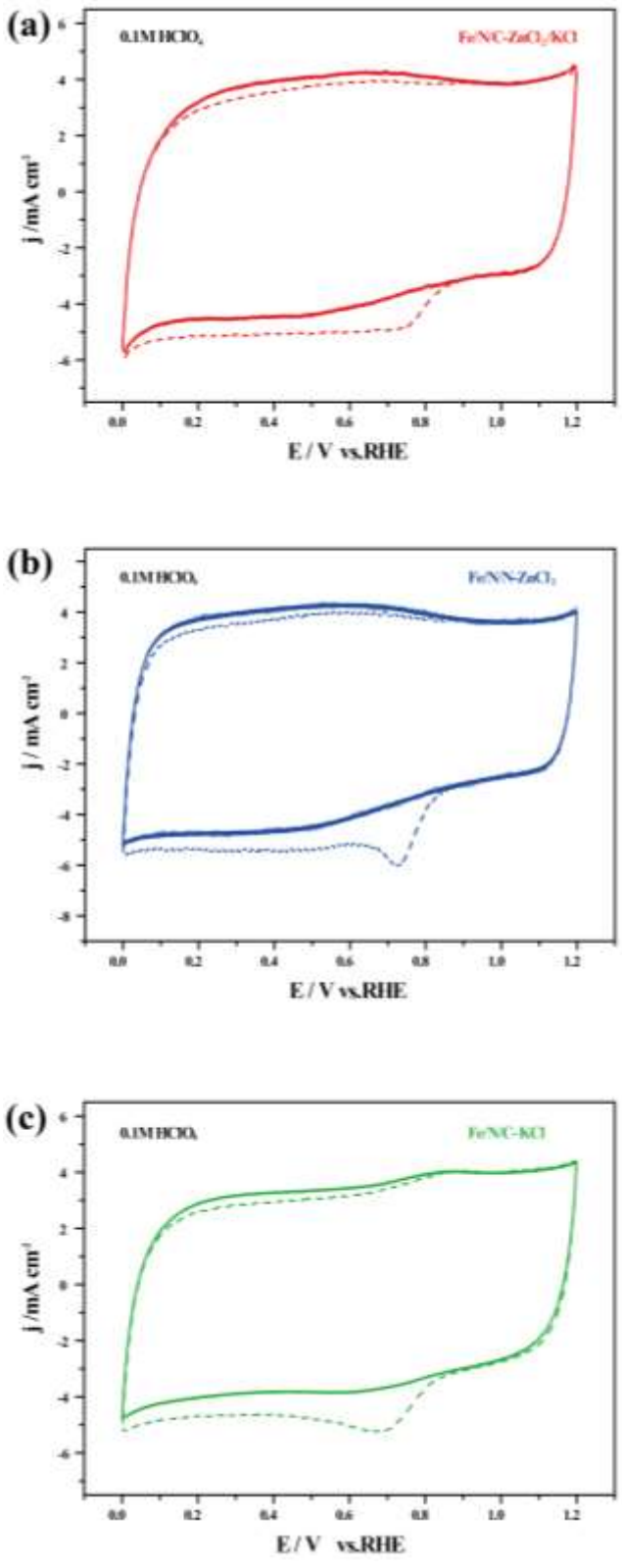

Figure S8. CV curves of (a) Fe/N/C-$ZnCl_2$/KCl, (b) Fe/N/C-$ZnCl_2$ and (c) Fe/N/C-KCl catalysts in N_2-saturated (solid line) and O_2-saturated (dotted line) 0.1 M $HClO_4$.

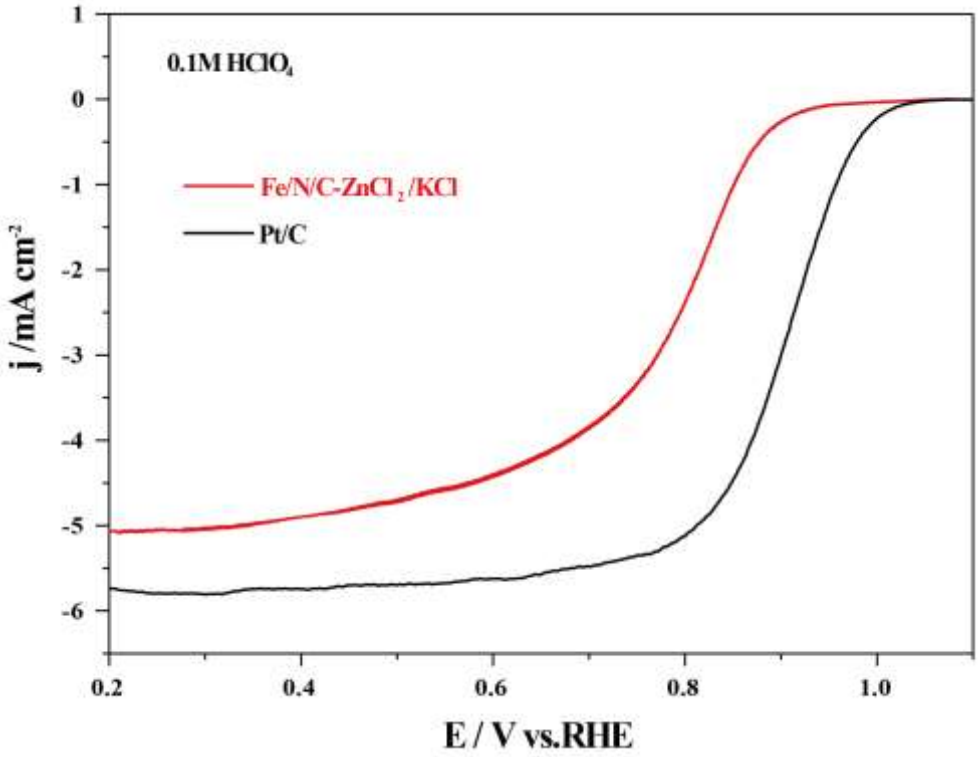

Figure S9. ORR polarization curves of Fe/N/C-$ZnCl_2$/KCl and Pt/C catalysts in O_2-saturated 0.1 M $HClO_4$ at a sweep rate of 10 mV s^{-1} and 1,600 rpm rotating speed.

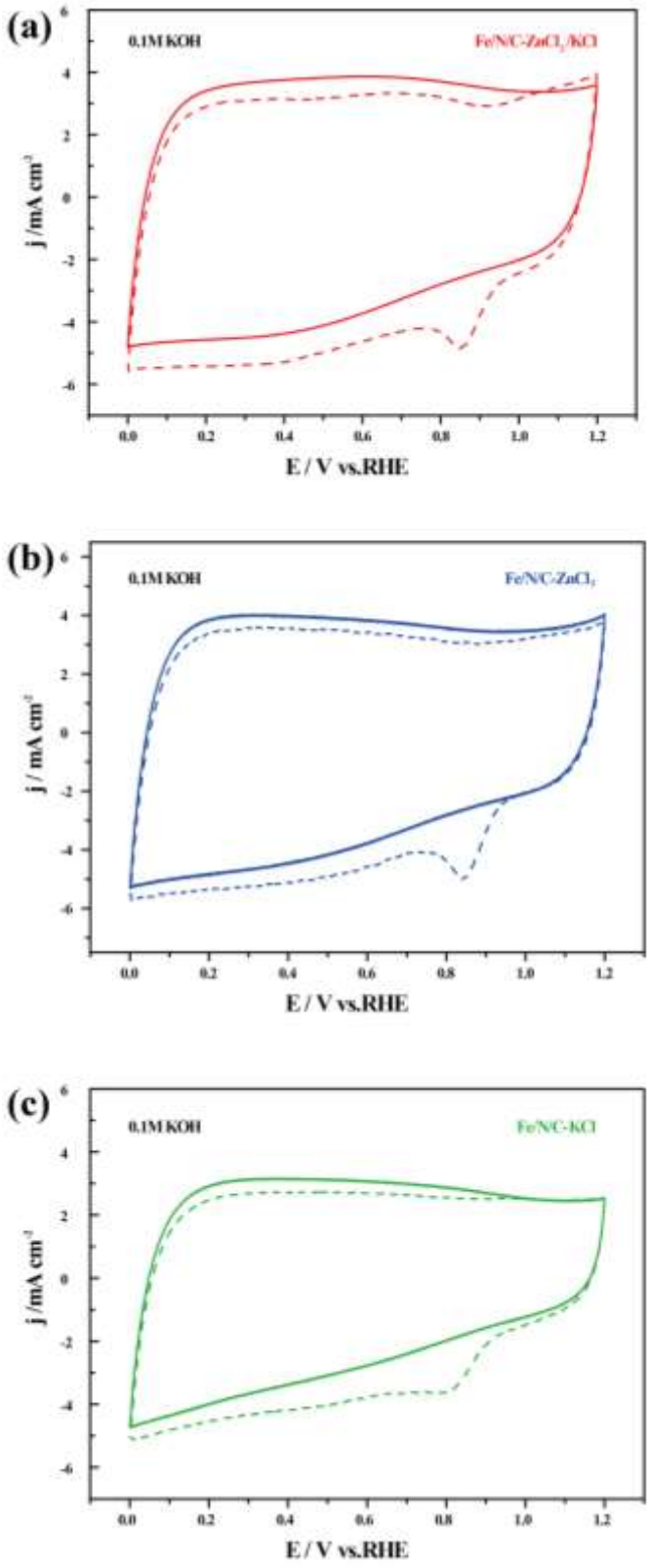

Figure S10. CV curves of (a) Fe/N/C-$ZnCl_2$/KCl, (b) Fe/N/C-$ZnCl_2$ and (c) Fe/N/C-KCl catalysts in N_2-saturated (solid line) and O_2-saturated (dotted line) 0.1 M KOH.

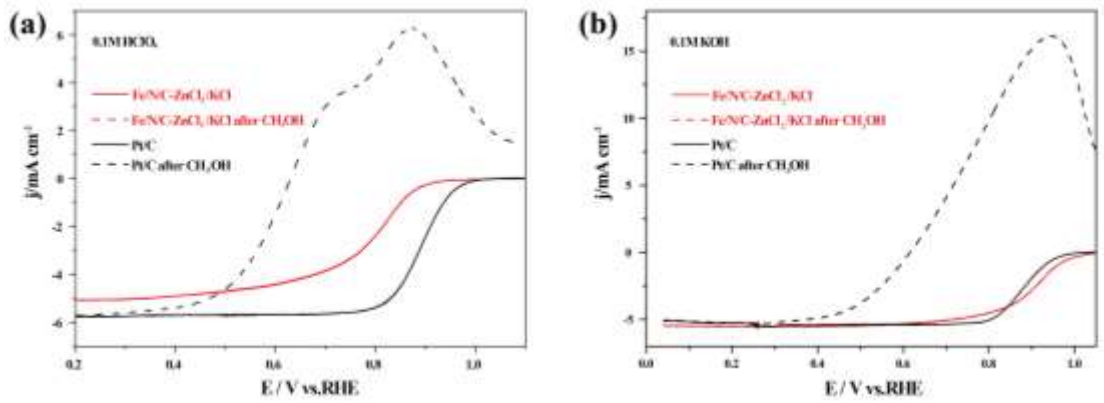

Figure S11. ORR polarization curves of Fe/N/C-$ZnCl_2$/KCl and Pt/C catalysts in O_2-saturated (a) 0.1 M $HClO_4$ and (b) 0.1 M KOH, and upon the addition of 0.5 M CH_3OH at a sweep rate of 10 mV s^{-1} and 1,600 rpm rotating speed.

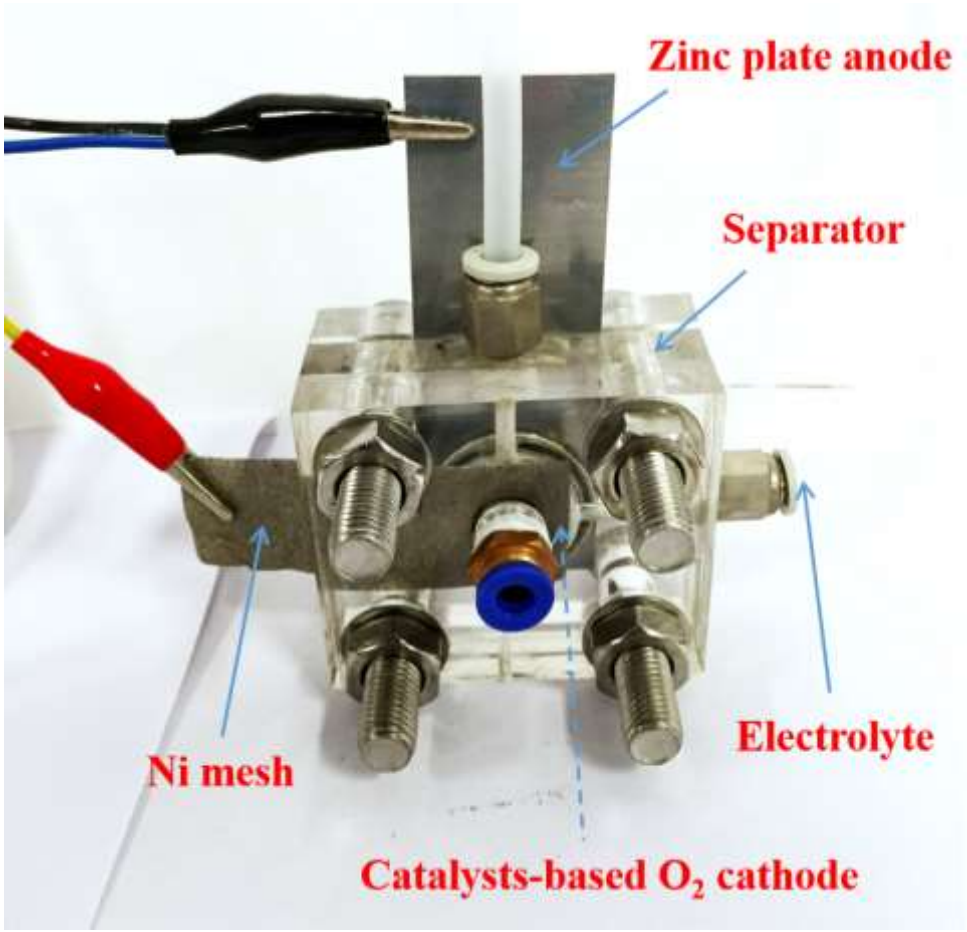

Figure S12. Optical picture of primary Zn-O_2 battery. The pure 6M KOH electrolyte was used as electrolyte for primary Zn-O_2 battery.

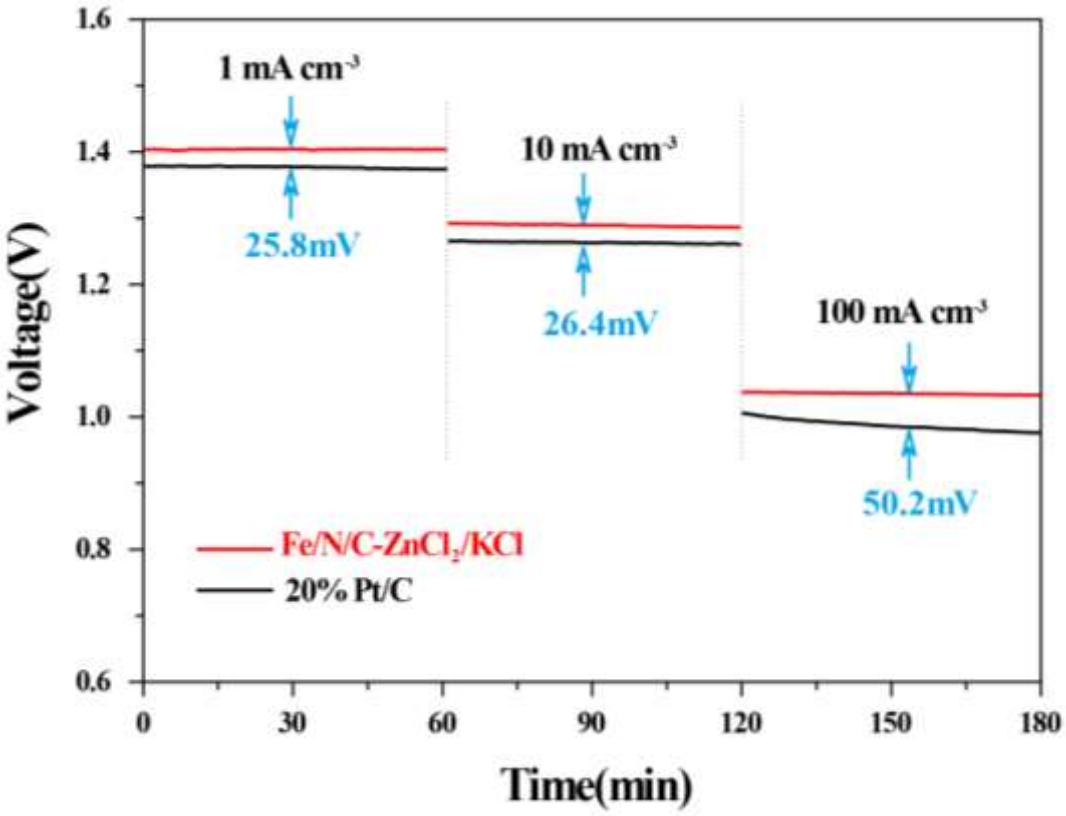

Figure S13. Galvanostatic discharge profile of Zn-O_2 batteries assembled with Fe/N/C-$ZnCl_2$/KCl and 20% Pt/C catalysts as cathode at different current densities.

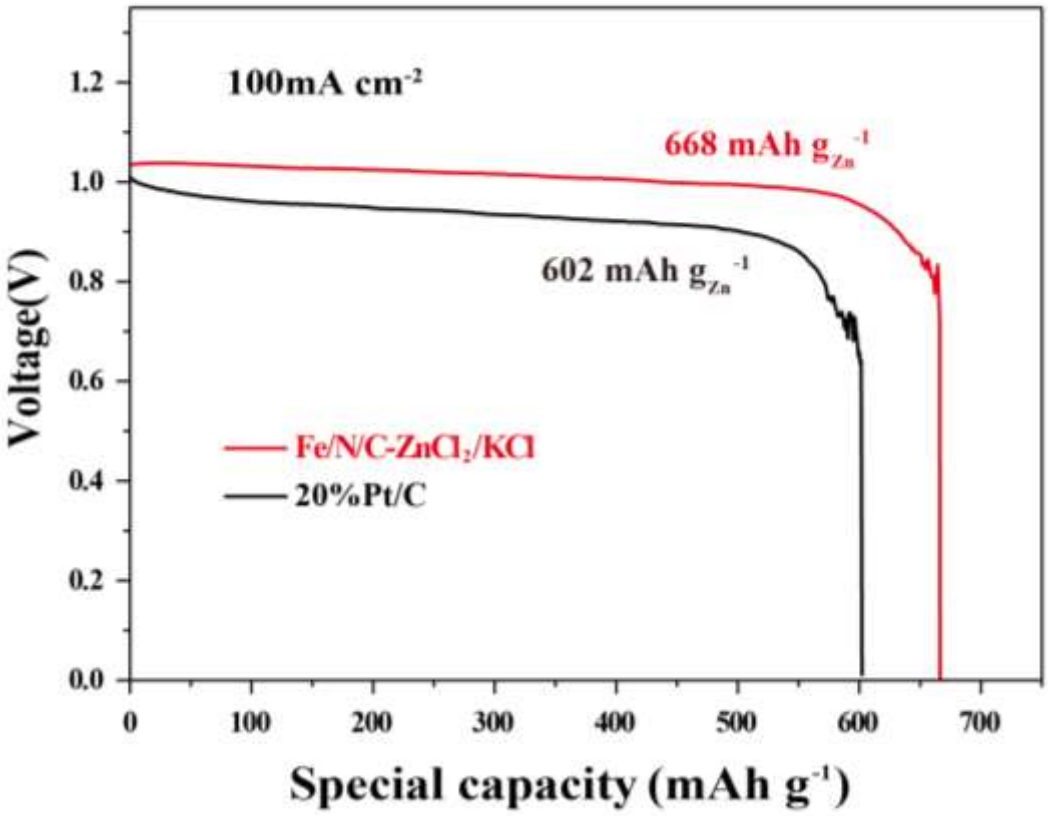

Figure S14. Discharge curves of Zn-O_2 batteries assembled with Fe/N/C-$ZnCl_2$/KCl and 20%Pt/C catalysts as cathode at 100 mA cm^{-2} discharging rate.

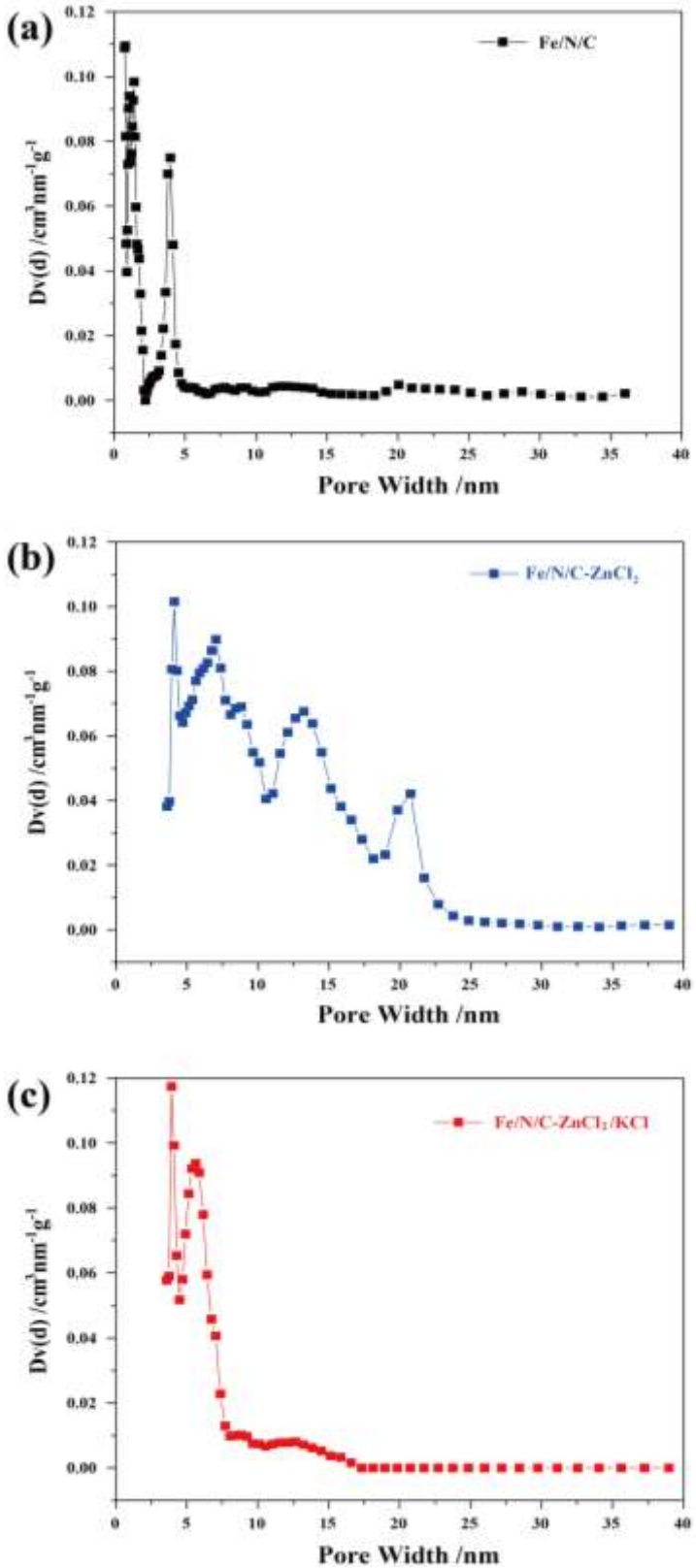

Figure S15. Quenched solid density functional theory (QSDFT) pore size distribution from N_2 (77K) adsorbed for Fe/N/C, Fe/N/C-$ZnCl_2$, Fe/N/C-$ZnCl_2$/KCl shown over a pore size range up to a pore width of 40nm.

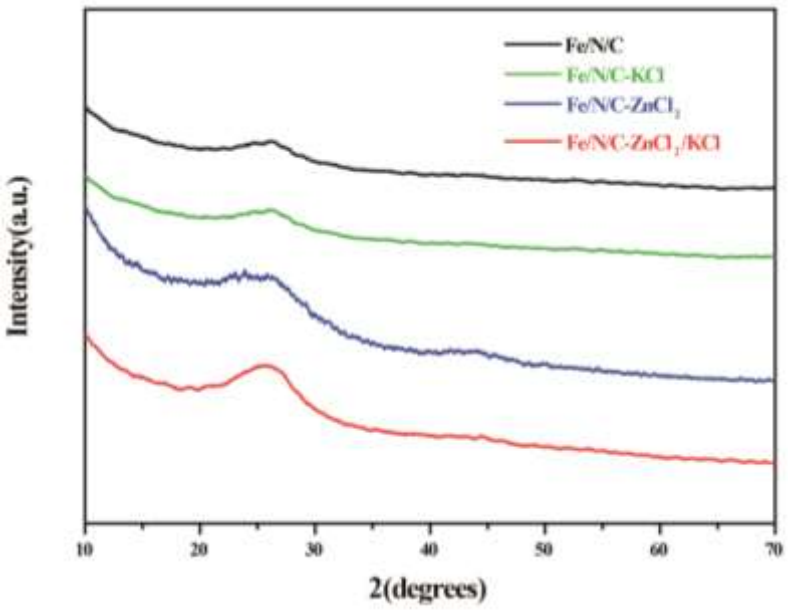

Figure S16. Powder X-ray diffraction patterns of the Fe/N/C, Fe/N/C-KCl, Fe/N/C-$ZnCl_2$, and Fe/N/C-$ZnCl_2$/KCl catalysts.

Table S1. Comparison of the element contents of Fe/N/C-$ZnCl_2$/KCl, Fe/N/C-$ZnCl_2$, Fe/N/C-KCl and Fe/N/C catalysts obtained from XPS and the Fe content obtained form ICP-MS.

Sample	C(at.%)	N(at.%)	O(at.%)	Fe(at.%)	ICP-MS Fe(wt%)
Fe/N/C-$ZnCl_2$/KCl	84.65	9.85	4.81	0.69	3.25
Fe/N/C-$ZnCl_2$	89.65	5.20	4.59	0.57	0.71
Fe/N/C-KCl	88.53	5.54	5.12	0.81	4.92
Fe/N/C	86.19	5.64	5.90	2.27	2.38

Table S2. Comparison of the nitrogen configurations of Fe/N/C-$ZnCl_2$/KCl, Fe/N/C-$ZnCl_2$, Fe/N/C-KCl and Fe/N/C catalysts.

Sample	Pyridinic-N/%	Fe-N_X/%	Pyrrolic-N/%	Quaternary-N/%	Oxidized-N/%
	~398.21eV	~399.57eV	~400.54eV	~401.20eV	~402.10eV
Fe/N/C-$ZnCl_2$/KCl	33.58	19.20	22.45	23.11	1.66
Fe/N/C-$ZnCl_2$	40.40	4.72	12.55	29.74	12.60
Fe/N/C-KCl	43.77	5.04	19.85	20.54	10.80
Fe/N/C	22.99	0.62	23.95	36.68	15.76

Table S3. The corresponding fitted parameters based on EIS of Fe/N/C-$ZnCl_2$/KCl, Fe/N/C-$ZnCl_2$ and Fe/N/C-KCl catalysts.

Sample	R_Ω	R_{ct}	R_d
Fe/N/C-$ZnCl_2$/KCl	28.60	187.63	151.20
Fe/N/C-$ZnCl_2$	27.50	208.09	849.54
Fe/N/C-KCl	30.00	752.68	569.18

Table S4. Comparison of the ORR activity of Fe/N/C-$ZnCl_2$/KCl catalyst with other reported electrocatalysts in both acidic and alkaline electrolytes.

Sample	$E_{1/2}$ (V vs. RHE) 0.1M $HClO_4$	$E_{1/2}$ (V vs. RHE) 0.1M KOH	Loading (μg cm^{-2})	Rotating rate (rpm)	Reference
NPMC-1000	~	0.85	150	1600	S1
Co@Co_3O_4@C–CM	~	0.81	100	1600	S2
PCN-FeCo/C	~	0.85	200	1600	S3
PCN-FeCo/C	0.76	~	600	1600	S3
Fe_3/C-800	~	0.83	600	900	S4
Fe_3/C-700	0.73	~	600	900	S4
FePhen@MOF-$ArNH_3$	0.79	0.86	600	1600	S5
FePhenMOF–$ArNH_3$	0.78	~	600	1600	S6
Co_3O_4/N-rmGO	~	0.83	100	1600	S7
P-CNCo-20	~	0.85	100	1600	S8
LDH@ZIF-67-800	~	0.83	200	1600	S9
Co,N-CNF	~	0.82	120	1600	S10
N-doped Fe/Fe_3C@graphitic layer/CNT	~	0.715	100	1600	S11
FePc/rGO	~	0.855	530	1600	S12
Atomically Dispersed Fe-N-C	~	0.85	600	1600	S13
Fe-N-CNT/PC	0.79	0.88	800	1600	S14
Fe_3C/NG-800	0.365	-0.444	600	1600	S15
Fe/N/C-$ZnCl_2$/KCl	**0.803**	**0.918**	**500**	**1600**	**This work**

Table S5. BET surface areas, pore volume of Fe/N/C-$ZnCl_2$/KCl, Fe/N/C-$ZnCl_2$, and Fe/N/C catalysts.

Sample	SBET(m^2g^{-1})	Pore volume (cm^3g^{-1})
Fe/N/C-$ZnCl_2$/KCl	1120	0.65
Fe/N/C-$ZnCl_2$	1883	1.32
Fe/N/C	346	0.38

References in Supporting Information

S1. J. T. Zhang, Z. H. Zhao, Z. H. Xia and L. M. Dai, *Nat. Nanotechnol.*, 2015, **10**, 444-452.

S2. W. Xia, R. Q. Zou, L. An, D. G. Xia and S. J. Guo, *Energy Environ. Sci.*, 2015, **8**, 568-576.

S3. Q. P. Lin, X. H. Bu, A. G. Kong, C. Y. Mao, F. Bu and P. Y. Feng, *Adv. Mater.*, 2015, **27**, 3431-3436.

S4. Y. Hu, J. O. Jensen, W. Zhang, L. N. Cleemann, W. Xing, N. J. Bjerrum and Q. F. Li, *Angew. Chem. Int. Ed.*, 2014, **53**, 3675-3679.

S5. K. Strickland, E. Miner, Q. Y. Jia, U. Tylus, N. Ramaswamy, W. T. Liang, M. T. Sougrati, F. Jaouen and S. Mukerjee, *Nat. Commun.*, 2015, **6**, 7343.

S6. J. K. Li, S. Ghoshal, W. T. Liang, M. T. Sougrati, F. Jaouen, B. Halevi, S. McKinney, G. McCool, C. Ma, X. Yuan, Z. F. Ma, S. Mukerjee and Q. Y. Jia, *Energy Environ. Sci.*, 2016, **9**, 2418-2432.

S7. Y. Y. Liang, Y. G. Li, H. L. Wang, J. G. Zhou, J. Wang, T. Regier and H. J. Dai, *Nat. Mater.*, 2011, **10**, 780-786.

S8. Y. Z. Chen, C. M. Wang, Z. Y. Wu, Y. J. Xiong, Q. Xu, S. H. Yu and H. L. Jiang, *Adv. Mater.*, 2015, **27**, 5010-5016.

S9. Z. H. Li, M. F. Shao, L. Zhou, R. K. Zhang, C. Zhang, M. Wei, D. G. Evans and X. Duan, *Adv. Mater.*, 2016, **28**, 2337-2344.

S10. L. Shang, H. J. Yu, X. Huang, T. Bian, R. Shi, Y. F. Zhao, G. I. N. Waterhouse, L. Z. Wu, C. H. Tung and T. R. Zhang, *Adv. Mater.*, 2016, **28**, 1668-1674.

S11. J. S. Li, S. L. Li, Y. J. Tang, M. Han, Z. H. Dai, J. C. Bao and Y. Q. Lan, *Chem. Commun.*, 2015, **51**, 2710-2713.

S12. T. Taniguchi, H. Tateishi, S. Miyamoto, K. Hatakeyama, C. Ogata, A. Funatsu, S. Hayami, Y. Makinose, N. Matsushita, M. Koinuma and Y. Matsumoto, *Part. Part. Syst. Charact.*, 2013, **30**, 1063-1070.

S13. P. Z. Chen, T. P. Zhou, L. L. Xing, K. Xu, Y. Tong, H. Xie, L. D. Zhang, W. S. Yan, W. S. Chu, C. Z. Wu and Y. Xie, *Angew. Chem. Int. Ed.*, 2017, **56**, 610-614.

S14. Y. J. Sa, D. J. Seo, J. Woo, J. T. Lim, J. Y. Cheon, S. Y. Yang, J. M. Lee, D. Kang, T. J. Shin, H. S. Shin, H. Y. Jeong, C. S. Kim, M. G. Kim, T. Y. Kim and S. H. Joo, *J. Am. Chem. Soc.*, 2016, **138**, 15046-15056.

S15. Z. Y. Wu, X. X. Xu, B. C. Hu, H. W. Liang, Y. Lin, L. F. Chen and S. H. Yu, *Angew. Chem. Int. Ed.*, 2015, **127**, 8297-8301.